

# Dyson-Schwinger equations and the muon $g-2$

Khépani Raya

*Departamento de Física Teórica y del Cosmos, Universidad de Granada, E-18071, Granada, Spain*

Adnan Bashir

*Instituto de Física y Matemáticas, Universidad Michoacana de San Nicolás de Hidalgo, Morelia, Michoacán 58040, Mexico*

Ángel S. Miramontes

*Instituto de Física y Matemáticas, Universidad Michoacana de San Nicolás de Hidalgo, Morelia, Michoacán 58040, Mexico*

Pablo Roig

*Departamento de Física, Centro de Investigación y de Estudios Avanzados del IPN,*

*Apdo. Postal 14-740,07000 Ciudad de México, Mexico*

Received XX YY 2021; accepted ZZ WW 2022

We present a brief introduction to the Dyson-Schwinger equations (DSEs) approach to hadron and high-energy physics. In particular, how this formalism is applied to calculate the electromagnetic form factors  $\gamma^*\gamma^* \rightarrow \mathbf{P}^0$  and  $\gamma^*\mathbf{P}^\pm \rightarrow \mathbf{P}^\pm$  (with  $\mathbf{P}^\pm$  and  $\mathbf{P}^0$  charged and neutral ground-state pseudoscalar mesons, respectively) is discussed. Subsequently, the corresponding contributions of those form factors to the muon anomalous magnetic moment ( $g - 2$ ) are estimated. We look forward to promoting the DSE approach to address theoretical aspects of the muon  $g - 2$ , highlighting some calculations that could be carried out in the future.

*Keywords:* Dyson-Schwinger equations, electromagnetic form factors, hadronic light-by-light contributions

*PACS:* 13.40.Em Electric and magnetic moments; 13.40.Gp Electromagnetic form factors; 11.10.St Bound and unstable states; Bethe-Salpeter equations

## 1. Introduction

The Standard Model (SM) of particle physics is supposed to describe ordinary matter in terms of elementary particles and their interactions. As a theory, the SM has been quite successful: continuous confrontation with empirical observations (experiment) reveals how robust it is. Even though it is sometimes difficult for it to explain some facts of Nature, such as confinement and dynamical mass generation in quantum chromodynamics (QCD) [1], only those quantities which require high precision measurements (or calculations) give us a small window to doubt the completeness of the SM to describe ordinary matter phenomena (aside from e.g. the origin of neutrino masses or the baryogenesis mechanism, which can be related to scales not directly accessible by current experiments). This is the case of the so called muon anomalous magnetic moment,  $a_\mu := (g_\mu - 2)/2$ . The historical discrepancy between experimental and theoretical values of  $a_\mu$  is fueled after the recent (first) measurement from the muon  $g - 2$  experiment at Fermilab (FNAL) [2]:

$$a_\mu^{\text{FNAL}} = 116592040(54) \times 10^{-11}, \quad (1)$$

which, in combination with the previous experiment at Brookhaven National Laboratory (BNL) [3], yields the accepted worldwide experimental average of:

$$a_\mu^{\text{Exp}} = 116592061(41) \times 10^{-11}. \quad (2)$$

Conversely, several theoretical efforts, orchestrated by the Muon  $g-2$  Theory Initiative, produce the following value as

the Standard Model prediction of this quantity [4]:

$$a_\mu^{\text{SM}} = 116591810(43) \times 10^{-11}. \quad (3)$$

Experiment so far has reached an amazing precision of 0.35 parts per million, and both SM and experiment exhibit the same level of accuracy; nevertheless,  $a_\mu^{\text{SM}}$  deviates  $4.2\sigma$  from  $a_\mu^{\text{Exp}}$ . While waiting for ongoing runs at FNAL and upcoming new experiments at J-PARC [5], one should inquire on this observable from the theoretical point of view. The degree of sophistication of the SM experiment and predictions (about  $a_\mu$ ), and more than anything, their discrepancy, excites those seeking explanations based on new physics. Either way, one must ensure that all contributions to  $a_\mu$  that come from the SM are included and carefully calculated, as well as that they have a sufficient degree of precision. The SM contributions to  $a_\mu$  are divided into those coming from quantum electrodynamics (QED), electroweak (EW) and hadronic contributions (at a fundamental level, QCD); the latter, further divided in hadronic vacuum polarization (HVP) and hadronic light-by-light (HLbL) contributions. Naturally, the QED part (calculated up to 5-loops) dominates [6],  $a_\mu^{\text{QED}} = 116584718.931(104) \times 10^{-11}$ . The EW contribution is subdominant but also well determined,  $a_\mu^{\text{EW}} = 153.6(1.0) \times 10^{-11}$  [7, 8]. On the other hand, the hadronic contributions saturate the error in the SM prediction (see [4, 9] and references therein):

$$a_\mu^{\text{HVP}} = 6845(40) \times 10^{-11}, \quad (4)$$

$$a_\mu^{\text{HLbL}} = 92(18) \times 10^{-11}. \quad (5)$$

It is not surprising that these are the least restricted contributions, demanding special attention. The non-perturbative nature of QCD often leads to difficulties not present in the QED-EW part of the SM. Thus, in evaluating the hadronic contributions to  $a_\mu$  it is typical to appeal to data-driven analyses, effective theories, and lattice QCD; *e.g.* [10–19]. Nevertheless, there is a mathematical framework that requires neither the experimental inputs of the data-driven approaches nor the computer power of lattice QCD: the Dyson-Schwinger equations (DSEs) formalism [20–22]. Even though there is a plethora of hadron physics predictions based upon this formalism (for example [23–32]), as well as recent and pioneering works on hadronic contributions to the muon  $g-2$  [33–38], little attention has been given to this approach as a valuable tool for muon  $g-2$  related studies.

In this manuscript, we revisit Refs. [33, 34], to briefly describe how to evaluate the HLbL  $\mathbf{P}^\pm$ -*box* contributions ( $\mathbf{P}^\pm = \pi^\pm, K^\pm$ ), given by the  $\gamma^* \mathbf{P}^\pm \rightarrow \mathbf{P}^\pm$  elastic form factors (EFFs), and the  $\mathbf{P}^0$ -*pole* contributions ( $\mathbf{P}^0 = \pi^0, \eta, \eta', \eta_c, \eta_b$ ), obtained from  $\gamma^* \gamma^* \rightarrow \mathbf{P}^0$  transition form factors (TFFs). The manuscript is organized as follows: Section 2 presents some general aspects for the description of mesons within the DSE framework. In Section 3, we discuss the calculation of EFFs and TFFs, presenting the obtained numerical results. Section 4 gathers such results and evaluates their contribution to  $a_\mu$ . Finally, Section 5 summarizes our findings and presents a vision about how the DSEs formalism can assist some theoretical aspects of the muon  $g-2$ .

## 2. The Dyson-Schwinger and Bethe-Salpeter equations approach

Essentially, the DSEs are the equations of motion in a quantum field theory; in this case, QCD. Every Green Function obeys a DSE which, in turn, requires the knowledge of at least one higher-order Green Function [20]. This forms an infinite tower of coupled (integral) equations which contains all the dynamics, therefore requiring a systematic truncation in order to extract the encoded physics [39, 40]. Notwithstanding, this formalism captures the perturbative and non-perturbative facets of QCD at once, thus being an ideal platform to investigate hadron properties.

That being said, let us start by recalling the DSE for the quark propagator:

$$S^{-1}(p) = Z_2[S^{(0)}(p)]^{-1} + \int_q^\Lambda K^{(1)}(q, p)S(q),$$

$$K^{(1)}(q, p) = \frac{4}{3}Z_1g^2D_{\mu\nu}(p-q)\gamma_\mu \otimes \Gamma_\nu(p, q), \quad (6)$$

where  $\int_q^\Lambda = \int \frac{d^4q}{(2\pi)^4}$  stands for a Poincaré invariant regularized integration, with  $\Lambda$  for the regularization scale. The rest of the pieces carry their usual meanings (color and flavor indices have been omitted for simplicity):

- $D_{\mu\nu}$  is the gluon propagator and  $g$  is the Lagrangian coupling constant.

- $\Gamma_\nu$  the fully-dressed quark-gluon vertex (QGV) which, in its full glory, is characterized by 12 Dirac structures [41–43] (some of them are explicitly connected with dynamical mass generation in QCD).
- $Z_{1,2}$  are the QGV and quark wave-function renormalization constants, respectively.

Herein,  $S^{(0)}$  denotes the bare quark propagator,

$$S^{(0)}(p) = [i\gamma \cdot p + m^{\text{bm}}]^{-1}, \quad (7)$$

where  $m^{\text{bm}}$  is the Lagrangian bare mass. The fully-dressed quark propagator is represented as

$$S(p) = Z(p^2)(i\gamma \cdot p + M(p^2))^{-1}, \quad (8)$$

in such a way that the non-perturbative effects of the strong interactions are captured in the dressing functions  $Z(p^2)$  and  $M(p^2)$ , in analogy with its bare counterpart. In fact, the mass function,  $M(p^2)$ , is enhanced (a couple hundred MeVs) in the infrared region, as a consequence of dynamical chiral symmetry breaking (DCSB) [1]. From all the functions appearing in Eq. (6), only the quark mass function is independent of the renormalization point  $\zeta$ .

The description of mesons is obtained from the Bethe-Salpeter equation (BSE) [28, 39]:

$$\Gamma_H(p; P) = \int_q^\Lambda K^{(2)}(q, p; P)\chi_H(q; P), \quad (9)$$

whose ingredients are defined as follows:

- $\Gamma_H$  corresponds to the Bethe-Salpeter amplitude (BSA),  $H$  labeling the type of meson, while  $\chi_H(q; P) = S(q_+)\Gamma_H(q; P)S(q_-)$  denotes the BS wavefunction (BSWF).
- $P$  is the total momentum of the bound state;  $q_+ := q + \eta P$  and  $q_- := q - (1 - \eta)P$ , with  $\eta \in [0, 1]$  defining the relative momentum.

The Dirac structure characterizing the BSA depends on the meson's quantum numbers. In particular, for a pseudoscalar meson  $\mathbf{P}$ :

$$\Gamma_{\mathbf{P}}(q; P) = \gamma_5[iE_{\mathbf{P}}(q; P) + \gamma \cdot PE_{\mathbf{P}}(q; P) + \gamma \cdot qG_{\mathbf{P}}(q; P) + q_\mu\sigma_{\mu\nu}P_\nu H_{\mathbf{P}}(q; P)], \quad (10)$$

where that amplitude attached to  $\gamma_5$ ,  $E_{\mathbf{P}}(q; P)$ , is dominant. Finally,  $K^{(2)}$  corresponds to two particle irreducible quark/antiquark scattering kernel, which expresses the interactions between the quark and antiquark within the bound-state. Both Eq. (6) and Eq. (9) require, in principle, the knowledge of infinitely many QCD's Green Functions. A truncation scheme must be then specified in order to arrive at a tractable problem. Symmetry principles establish that, in fact,  $K^{(1)}$  and  $K^{(2)}$  are connected via vector and axial-vector Ward-Green-Takahashi identities (WGTIs) [44–46];

the vector WGTI entails electric charge conservation, while the axial-vector one implies the appearance of pions (light pseudoscalars) as the Goldstone bosons of DCSB [47].

Once a systematic truncation is chosen, the meson mass and BSWF are obtained from solutions of Eqs. (6) and (9); furthermore, the pseudoscalar meson leptonic decay constant ( $f_{\mathbf{P}}$ ) can be computed straightforwardly from the canonically normalized BSWF as:

$$f_{\mathbf{P}} P_{\mathbf{P}} = \text{tr}_{CD} Z_2 \int_q \gamma_5 \gamma_\mu \chi_{\mathbf{P}}(q; P), \quad (11)$$

where tr indicates the trace over color and Dirac indices. In the next section we briefly explain some sensible truncations for ground-state pseudoscalar mesons, employed in subsequent calculations.

### 2.1. Rainbow Ladder truncation

The simplest truncation that fullfills vector and axial-vector WGTIs is defined by the kernel ( $\{t, u, r, s\}$  color indices):

$$[K_{tu}^{rs}]^{\text{RL}}(q, p; P) = -\frac{4}{3} Z_2^2 D_{\mu\nu}^{\text{eff}}(p-q) [\gamma_\mu]_{ts} \otimes [\gamma_\nu]_{ru}, \quad (12)$$

which relate the 1-body and 2-body kernels as:

$$K^{(2)}(q, p; P) = K^{\text{RL}}(q, p; P) = -K^{(1)}(q, p; P). \quad (13)$$

This truncation is dubbed as the RL truncation [47]; a sensible and practical approach so long as we restrain ourselves to ground-state pseudoscalar and vector mesons [26, 29, 30, 48]. It is worth noticing that the gluon propagator has been promoted to an effective one,  $g D_{\mu\nu} \rightarrow D_{\mu\nu}^{\text{eff}}$ , where:

$$D_{\mu\nu}^{\text{eff}}(k) = \left( \delta_{\mu\nu} - \frac{k_\mu k_\nu}{k^2} \right) \mathcal{G}(k^2). \quad (14)$$

Herein,  $\mathcal{G}(k^2)$  captures all the missing information from the rich structure of  $\Gamma_\nu$ , lost after reducing  $\Gamma_\nu \rightarrow \gamma_\nu$ . Typically, we appeal to lattice QCD or phenomenological models to provide a sound representation for  $\mathcal{G}(k^2)$  [49–51]. Throughout this work, we shall employ the so called Qin-Chang (QC) interaction [51]. Avoiding details, the QC model is defined once the strength parameter,  $m_G = (wD)^{1/3}$ , is fixed to produce the masses and decay constants of the ground-state pseudoscalar mesons. Typical RL parameters are  $m_G \sim 0.8$  GeV and  $w \sim 0.5$  GeV; herein, the later is varied within the range  $w \in (0.4, 0.6)$  to estimate model uncertainties.

### 2.2. Beyond RL: Anomaly kernel

In discussing the  $\eta - \eta'$  states, it is convenient to work with a flavor basis, such that the associated Bethe-Salpeter amplitudes can be expressed as ( $l = u = d$ ):

$$\Gamma_{\eta, \eta'}(k; P) = \text{diag}(1, 1, 0) \Gamma_{\eta, \eta'}^l(k; P) \quad (15)$$

$$+ \text{diag}(0, 0, \sqrt{2}) \Gamma_{\eta, \eta'}^s(k; P). \quad (16)$$

<sup>1</sup> MCEs are also expected to play a major role in the description of nucleon and hyperon transition form factors, around  $Q^2 \approx 0$  [58–61].

Following Refs. [46, 52], the effects of the non-Abelian anomaly, not present in  $K^{\text{RL}}$  alone, are introduced at the level of the Bethe-Salpeter kernel ( $k = p - q$ ):

$$[K_{tu}^{rs}]^A(q, p; P) = -\mathcal{G}_A(k^2) (\sin^2 \theta_\xi [\mathbf{r} \gamma_5]_{rs} [\mathbf{r} \gamma_5]_{tu}) \quad (17)$$

$$+ \frac{1}{\chi_l^2} \cos^2 \theta_\xi [\mathbf{r} \gamma_5 \gamma \cdot P]_{rs} [\mathbf{r} \gamma_5 \gamma \cdot P]_{tu},$$

where  $\chi_l = M_l(0)$ , and  $\theta_\xi$  controls the relative strength between the  $\gamma_5$  and  $\gamma_5 \gamma \cdot P$  terms;  $\mathbf{r} = \text{diag}(1, 1, \nu_R)$  and  $\nu_R = M_l(0)/M_s(0) = 0.57$ . The strength and momentum dependence of the anomaly is controlled by

$$\mathcal{G}_A(k^2) = \frac{8\pi^2}{\omega_\xi^4} D_\xi \exp[-k^2/\omega_\xi^2]. \quad (18)$$

Thus, the 2-body kernel for the  $\eta - \eta'$  case becomes:

$$K^{(2)}(q, p; P) = K^{\text{RL}}(q, p; P) + K^A(q, p; P). \quad (19)$$

The new parameters,  $\{D_\xi, \omega_\xi, \cos^2 \theta_\xi\}$ , are fixed to provide a fair description of  $m_{\eta, \eta'}$  and  $J_{\eta, \eta'}^{l, s}$  [34, 52].

### 2.3. Beyond RL: Meson cloud effects

The interaction of a photon with a quark, the quark-photon vertex (QPV), is described by an inhomogeneous BSE:

$$\Gamma_\mu^f(p; P) = \gamma_\mu + \int_q^\Lambda K^{(2)}(q, p; P) \chi_\mu^f(q; P), \quad (20)$$

where  $\Gamma_\mu^f$  represents the QPV, the interaction of a photon with a  $f$ -flavor quark;  $\chi_\mu^f(q; P)$  is simply the unamputated vertex, which reads:

$$\chi_\mu^f(q; P) = S^f(q_+) \Gamma_\mu^f(q; P) S^f(q_-). \quad (21)$$

In the RL truncation, bound-states obtained from the homogeneous BSE, Eq. (9), appear as poles in the time-like axis. By corollary, solutions of Eq.(20) exhibit poles at  $Q^2 = -m_n^2$  [53] (herein,  $m_n$  corresponds to vector meson masses, such that  $m_1 = m_\rho$ ). This is an appreciated feature for space-like form factors; in particular, charge radii are obtained with better accuracy [53, 54]. In the case of the  $\gamma^* \gamma^*$  TFFs, Eq. (20) also guarantees that the abelian anomaly is faithfully reproduced [35, 55]. This makes the RL truncation of QCD's DSE a sound treatment to estimate the  $\mathbf{P}^\pm$ -box and  $\mathbf{P}^0$ -pole contributions: only a relatively small space-like region of the corresponding form factors actually matters for determining their contribution to  $a_\mu$  [34, 36].

It is worth exploring, however, what information a proper treatment of the time-like region could provide. The truncation introduced in Refs. [56, 57], denoted herein as BRL, takes into account resonance effects, thus shifting the vector-meson poles to the complex plane; subsequently, meson cloud effects (MCEs) are incorporated in the description of

the pion EFF<sup>1</sup>. These explorations have been adapted in [33] to compute the  $\pi - K$  EFFs and corresponding box contributions; in this case, the QC interaction model demands  $m_G \sim 0.84$  and  $\omega \in (0.6, 0.8)$  GeV to accurately produce  $m_{\pi, K}$  and  $f_{\pi, K}$ .

### 3. Electromagnetic form factors

Let us now focus on the calculation of the electromagnetic elastic and transition form factors,  $\gamma^* \mathbf{P}^\pm \rightarrow \mathbf{P}^\pm$  and  $\gamma^* \gamma^* \rightarrow \mathbf{P}^0$ , respectively.

#### 3.1. Elastic form factors

The electromagnetic process  $\gamma^* \mathbf{P}^\pm \rightarrow \mathbf{P}^\pm$  is described by a single form factor,  $F_{\mathbf{P}^\pm}(Q^2)$ . In the impulse approximation, which corresponds to a triangle diagram and is self consistent with the RL truncation [54],  $F_{\mathbf{P}^\pm}(Q^2)$  is obtained from [30]:

$$2K_\mu F_{\mathbf{P}^\pm}(Q^2) = e_u [F_{\mathbf{P}^\pm}^u(Q^2)]_\mu + e_{\bar{h}} [F_{\mathbf{P}^\pm}^{\bar{h}}(Q^2)]_\mu, \quad (22)$$

where  $\mathbf{P}^\pm$  is a  $u\bar{h}$  meson and  $e_{u, \bar{h}}$  are the electric charges of the quark and antiquark, respectively.  $[F_{\mathbf{P}^\pm}^f(Q^2)]_\mu$  denotes the interaction of the photon with a valence constituent  $f$ -in- $\mathbf{P}^\pm$ , such that:

$$\begin{aligned} [F_{\mathbf{P}^\pm}^f(Q^2)]_\mu &= \text{tr}_{CD} \int_q \chi_\mu^f(q + p_f, q + p_i) \\ &\times \Gamma_{\mathbf{P}^\pm}(q_i; p_i) S(q) \Gamma_{\mathbf{P}^\pm}(q_f; -p_f). \end{aligned} \quad (23)$$

The kinematics is defined as follows:  $p_{i, f} = K \mp Q/2$  and  $q_{i, f} = q + p_{i, f}/2$ , such that  $p_{i, f}^2 = -m_{\mathbf{P}^\pm}^2$ ; naturally,  $m_{\mathbf{P}^\pm}$  is the mass of the pseudoscalar meson and  $Q$  the photon momentum. Beyond RL, Eq. (23) might be supplemented by additional terms [54], and so is the case of the BRL truncation. Thus, in principle, all the necessary ingredients for the computation of  $F_{\mathbf{P}^\pm}(Q^2)$  have been gathered.

For future references, and having made use of Eq. (20) to define the QPV, we will name this approach the *direct computation*. This usual procedure was employed in Refs. [35, 36] for the calculation of  $\pi - K$  EFFs and corresponding box contributions, albeit in the RL truncation with the Maris-Tandy (MT) model [62].

#### 3.2. Transition form factors

The transition  $\gamma^* \gamma^* \rightarrow \mathbf{P}^0$  is also described by a single form factor,  $G_{\mathbf{P}^0}(Q_1^2, Q_2^2, Q_1 \cdot Q_2)$ . In the impulse approxima-

tion [29]:

$$\begin{aligned} \mathcal{T}_{\mu\nu}(Q_1, Q_2) &= T_{\mu\nu}(Q_1, Q_2) + T_{\nu\mu}(Q_2, Q_1), \quad (24) \\ T_{\mu\nu}(Q_1, Q_2) &= \frac{1}{4\pi^2} \epsilon_{\mu\nu\alpha\beta} Q_{1\alpha} Q_{2\beta} G_{\mathbf{P}^0}(Q_1^2, Q_2^2, Q_1 \cdot Q_2) \\ &= \mathbf{e}_{\mathbf{P}^0}^2 \text{tr}_{CD} \int_q i\chi_\mu^f(q, q_1) \Gamma_{\mathbf{P}^0}(q_1, q_2) \\ &\times S_f(q_2) i\Gamma_\nu^f(q_2, q), \quad (25) \end{aligned}$$

where  $Q_1, Q_2$  are photon momenta, and the kinematics is set by:  $(Q_1 + Q_2)^2 = P^2 = -m_{\mathbf{P}^0}^2$ ,  $q_1 = q + Q_1$ ,  $q_2 = q - Q_2$ ; finally,  $\mathbf{e}_{\mathbf{P}^0}$  is a factor associated with the electric charges of the valence quark/antiquark<sup>2</sup>. As for the EFFs, the calculation of TFFs requires the knowledge of the quark propagators, BSAs and QPV. This exhibits how, within the DSE formalism, hadronic observables maintain a traceable connection with QCD's fundamental ingredients.

A direct computation can be performed at this stage. Nevertheless, technical reasons restrict the evaluation of the form factors to a limited domain of space-like momenta. For instance, the pion elastic and single of shell TFFs can only be obtained up to  $Q^2 \sim 4$  GeV<sup>2</sup> [54, 55], without appealing to sophisticated mathematical techniques for extrapolation [63]. The domain in which a direct computation of the form factors is possible is sufficient to accurately estimate their corresponding contributions to  $a_\mu$ . However, we also present an alternative technique, based upon perturbation theory integral representations (PTIRs) [29–31], to evaluate the form factors at arbitrarily large momenta. Among other things, this allows us to take into account the asymptotic behavior of the form factors when proposing parametric representation for the numerical data, particularly relevant in the case of TFFs [12, 34, 64].

#### 3.3. The PTIR approach

A practical perturbation theory integral representation for the quark propagators and BSAs was put forward in [30, 31], to calculate the pion distribution amplitude and space-like EFF. The general idea, which applies to all pseudoscalars [29, 52, 65], is to describe the quark propagators in terms of  $j_m = 2$  complex conjugate poles (CCPs), and express the BSAs,  $\mathcal{A}_j(k; P)$ , as follows:

$$\mathcal{A}_j(k; P) = \sum_{i=1}^{i_n} \int_{-1}^1 dw \rho_i^j(w) \frac{c_i^j (\Lambda_{i,j}^2)^{\beta_i^j}}{(k^2 + wk \cdot P + \Lambda_{i,j}^2)^{\alpha_i^j}}. \quad (26a)$$

The interpolation parameters  $\{z_j, m_j\}$ ,  $\{\alpha_i^j, \beta_i^j, \Lambda_{i,j}, c_i^j, i_n = 3\}$  (for quark propagators and BSAs, respectively), as well as the spectral weights,  $\rho_i^j(w)$ , are determined through fitting to the numerical results of the corresponding DSE-BSEs. The sets of parameters are found through Refs. [33, 34, 66].

<sup>2</sup> Eq. (25) must be adapted to account for the flavour decomposition of the  $\eta - \eta'$  systems [52].

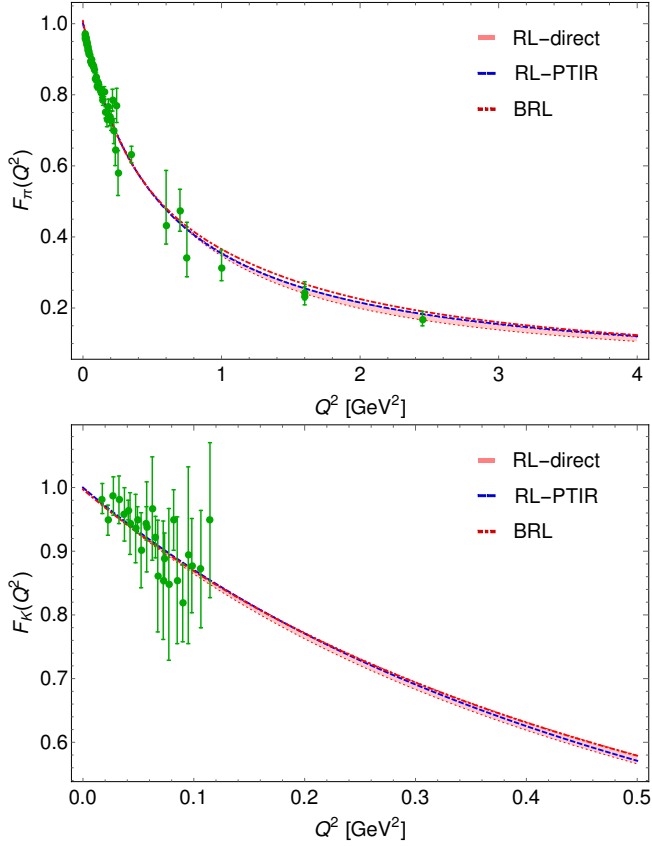


FIGURE 1.  $\pi^+$  and  $K^+$  EFFs. The band in the RL-direct result accounts for the variation of the QC model parameters, as described in text; those corresponding to the PTIR and BRL results are not shown, since there is a considerable overlap. The charge radii,  $r_\pi = 0.676(5)$  fm and  $r_K = 0.595(5)$  fm are practically insensitive to the model inputs and truncation. Experimental data from Refs. [67–70].

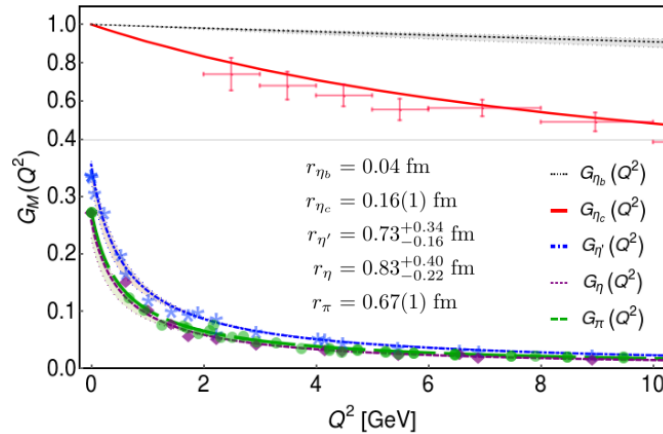


FIGURE 2. Single off-shell  $\gamma\gamma^* \rightarrow \mathbf{P}^0$  TFFs and corresponding charge radii [25]. Experimental data is taken from [16] and references therein. The mass units are in GeV.

<sup>3</sup> The quark propagator is written as  $S(p) = -i\gamma \cdot p \sigma_v(p^2) + \sigma_s(p^2)$ , with  $\sigma_{s,v}(p^2)$  being algebraically related to  $M(p^2)$  and  $Z(p^2)$  in Eq. (8).

Constructing a PTIR for the QPV in Eq. (20) turns out to be difficult and unpractical [48]. Thus, appealing to gauge covariance properties [71], the following Ansatz has been proposed and systematically tested [29, 52, 65]:

$$\begin{aligned} \chi_\mu(k_f, k_i) = & \gamma_\mu \Delta_{k^2 \sigma_V} \\ & + [\mathbf{s}\gamma \cdot k_f \gamma_\mu \gamma \cdot k_i + \bar{\mathbf{s}}\gamma \cdot k_i \gamma_\mu \gamma \cdot k_f] \Delta_{\sigma_V} \\ & + [\mathbf{s}(\gamma \cdot k_f \gamma_\mu + \gamma_\mu \gamma \cdot k_i) \\ & + \bar{\mathbf{s}}(\gamma \cdot k_i \gamma_\mu + \gamma_\mu \gamma \cdot k_f)] i \Delta_{\sigma_S}, \end{aligned} \quad (27)$$

where  $\Delta_F = [F(k_f^2) - F(k_i^2)] / (k_f^2 - k_i^2)$ ,  $\bar{\mathbf{s}} = 1 - \mathbf{s}$ . Up to transverse pieces associated with  $\mathbf{s}$ ,  $\chi_\mu(k_f, k_i)$  and  $S(k_f)\Gamma_\mu(k_f, k_i)S(k_i)$  are equivalent. The transverse terms are weighted by the function  $\mathbf{s}(Q_1^2, Q_2^2)$ , which is exponentially suppressed and tuned to reproduce the empirical decay widths [34]; as a by-product, the effects of the  $\rho$ -meson pole in the low- $Q^2$  domain are properly mimicked.

Defined as in Eq. (27) - flavor labels omitted on purpose, the QPV is expressed in terms of the quark propagator dressing functions<sup>3</sup>. With all the ingredients in Eqs. (22, 23, 25) expressed in a PTIR, the evaluation of the 4-momentum integral follows after a series of standard algebraic steps (numerical integration is only carried out for the Feynman parameters and spectral weights). Hence, the form factors can be calculated at arbitrarily large space-like momenta.

## 4. Numerical Results and HLbL contributions

### 4.1. Elastic and transition factors

The  $\pi$  and  $K$  EFFs are presented in Fig. 1. We compare the RL results which follow from the direct computation and PTIR approach; the compatibility between both calculations is evident. In the depicted domain, the BRL truncation yields similar outcomes. Furthermore, our obtained EFFs are in clear agreement with the DSE results reported in Ref. [36]. TFFs are presented in Fig. 2, in the single off-shell case. The agreement of those form factors with the available experimental data is clear. Notably, the PTIR approach enabled us to calculate the  $\eta_c$  and  $\eta_b$  TFFs without facing new obstacles.

### 4.2. Charged pion and kaon pole contributions

To calculate the  $\mathbf{P}^\pm$ -box contributions, we employ the master formula derived in [17], which reads:

$$\alpha_\mu^{\mathbf{P}\text{-box}} = \frac{\alpha_{em}^3}{432\pi^2} \int_\Omega \sum_i^{12} T_i(Q_1, Q_2, \tau) \bar{\Pi}_i^{\mathbf{P}\text{-box}}(Q_1, Q_2, \tau), \quad (28)$$

where  $\alpha_{em}$  is the QED coupling constant, and

$$\int_\Omega := \int_0^\infty d\tilde{\Sigma} \tilde{\Sigma}^3 \int_0^1 dr r \sqrt{1-r^2} \int_0^{2\pi} d\phi. \quad (29)$$

The functions  $\bar{\Pi}_i^{\mathbf{P}^0\text{-box}}$  are expressed as:

$$\bar{\Pi}_i^{\mathbf{P}^0\text{-box}}(Q_1^2, Q_2^2, Q_3^2) = F_{\mathbf{P}}(Q_1^2)F_{\mathbf{P}}(Q_2^2)F_{\mathbf{P}}(Q_3^2) \times \frac{1}{16\pi^2} \int_0^1 dx \int_0^{1-x} dy I_i(x, y). \quad (30)$$

The scalar functions  $T_i$  and  $I_i$  are provided in Appendices B and C of Ref. [17], respectively. With the EFFs obtained in the RL truncation (direct and PTIR) and BRL, the numerical estimates for the  $\pi^\pm$ -box contributions are:

$$\begin{aligned} a_\mu^{\pi^\pm\text{-box}} &= -(15.4 \pm 0.3) \times 10^{-11} \text{ [RL-direct]}, \\ a_\mu^{\pi^\pm\text{-box}} &= -(15.6 \pm 0.3) \times 10^{-11} \text{ [RL-PTIR]}, \\ a_\mu^{\pi^\pm\text{-box}} &= -(15.7 \pm 0.2) \times 10^{-11} \text{ [BRL]}. \end{aligned} \quad (31)$$

Analogous results for the  $K^\pm$  case yield:

$$\begin{aligned} a_\mu^{K^\pm\text{-box}} &= -(0.47 \pm 0.03) \times 10^{-11} \text{ [RL-direct]}, \\ a_\mu^{K^\pm\text{-box}} &= -(0.48 \pm 0.03) \times 10^{-11} \text{ [RL-PTIR]}, \\ a_\mu^{K^\pm\text{-box}} &= -(0.48 \pm 0.02) \times 10^{-11} \text{ [BRL]}. \end{aligned} \quad (32)$$

From Fig. 1 and the above estimates, it is clear that the direct and PTIR approach are plainly compatible; the BRL truncation also yields similar outcomes. Therefore, one can combine the estimates in Eqs. (31)-(32) to produce the weighted averages:

$$a_\mu^{\pi^\pm\text{-box}} = -(15.6 \pm 0.2) \times 10^{-11}, \quad (33)$$

$$a_\mu^{K^\pm\text{-box}} = -(0.48 \pm 0.02) \times 10^{-11}, \quad (34)$$

where the errors reflect model and truncation uncertainties.

### 4.3. Pseudoscalar pole contributions

The master formula for the  $\mathbf{P}^0$ -pole contributions is found in Refs. [15, 64]. It is highly convenient to parameterize the numerical results of the TFFs in a sensible way. For the light pseudoscalars,  $\{\pi^0, \eta, \eta'\}$ , a Canterbury approximants representation turns out to be quite adequate [12]; with proper care, it captures all the short- and long distance facets of the TFFs [34]. Those form factors are then represented as ( $x = Q_1^2, y = Q_2^2$ ):

$$G_{\mathbf{P}}^{\text{light}}(x, y) = \frac{a_{00} + a_{10}(x + y) + a_{01}(xy)}{1 + b_{10}(x + y) + b_{01}(xy) + b_{11}(x + y)(xy)},$$

where the independent parameters,  $b_{i,j}$ , are fitted to the numerical data ( $a_{i,j}$  are fixed by the axial anomaly and short-distance QCD constraints, properly captured by the actual numerical solutions). The hardness of the  $\{\eta_c, \eta_b\}$  TFFs demands a much simpler representation. All interpolation parameters are listed in [34]. Finally, the corresponding  $\mathbf{P}^0$ -pole

contributions are:

$$\begin{aligned} a_\mu^{\pi^0\text{-pole}} &= (61.4 \pm 0.21) \times 10^{-11}, \\ a_\mu^{\eta\text{-pole}} &= (14.7 \pm 0.19) \times 10^{-11}, \\ a_\mu^{\eta'\text{-pole}} &= (13.6 \pm 0.08) \times 10^{-11}, \\ a_\mu^{\eta_c\text{-pole}} &= (0.9 \pm 0.1) \times 10^{-11}, \\ a_\mu^{\eta_b\text{-pole}} &= (0.26 \pm 0.01) \times 10^{-13}. \end{aligned} \quad (35)$$

Summing up the results from (35):

$$a_\mu^{\mathbf{P}^0\text{-pole}} = (90.6 \pm 4.9) \times 10^{-11}, \quad (36)$$

where the errors, accounting for model uncertainties (mostly dominated by the QPV Ansatz), have been added linearly.

## 5. Conclusions and scope

We described the computation of the electromagnetic form factors  $\gamma^*\mathbf{P}^\pm \rightarrow \mathbf{P}^\pm$  and  $\gamma^*\gamma^* \rightarrow \mathbf{P}^0$ , within the DSE approach to QCD, aiming to evaluate their contributions to  $a_\mu$ .

The EFFs were obtained, firstly, in the RL truncation. Direct computations and the PTIR approach were shown to be fully compatible, while also being in agreement with the DSE results from Refs. [35, 36]. It was also confirmed that the BRL truncation, which incorporates MCEs<sup>4</sup>, produces similar EFFs in the relevant domain for  $a_\mu$ ; the value of the latter being barely affected by the new effects in the truncation. Our most recent analysis, [33], supports these observations.

The validity of the PTIR approach is also manifested in the case of the  $\gamma^*\gamma^* \rightarrow \{\pi^0, \eta, \eta', \eta_c, \eta_b\}$  TFFs, whose calculation has been summarized herein and described in detail through Refs. [29, 34, 52, 65]. Our  $\{\pi^0, \eta, \eta'\}$  computations are fully compatible with those from [35, 63], even though the dealing with the non-Abelian anomaly is vastly different. Interestingly, our numerical results suggest a sizeable contribution from the  $\eta_c$  meson, which might be worth exploring in the future.

In this manuscript we have briefly discussed the capabilities of the DSE formalism to address calculations of hadronic observables, highlighting some quantities of interest for the muon  $g - 2$ . We hope to continue developing calculations related to the subject. For instance, following the remarks from [13], the contribution from axial-vector mesons is worth exploring, even though it represents a major computational challenge; on the other hand, estimating the contribution from excited pseudoscalars is within reach.

## 6. Acknowledgements

The authors acknowledge support from CONACYT and Cátedras Marcos Moshinsky (Fundación Marcos Moshinsky). This research was also partly supported by Coordinación de la Investigación Científica (CIC) of the University of Michoacán, Mexico, through Grant No. 4.10. KR wishes to acknowledge J. Rodríguez-Quintero for his valuable scientific counselling.

<sup>4</sup> The MCEs take place in the neighborhood of  $Q^2 \approx 0$  [58–60], such that, for increasing  $Q^2$ ,  $\text{BRL} \rightarrow \text{RL}$ .

1. Craig D. Roberts. On Mass and Matter. *AAPPS Bull.*, 31:6, 2021.
2. B. Abi et al. Measurement of the Positive Muon Anomalous Magnetic Moment to 0.46 ppm. *Phys. Rev. Lett.*, 126(14):141801, 2021.
3. G. W. Bennett et al. Final Report of the Muon E821 Anomalous Magnetic Moment Measurement at BNL. *Phys. Rev. D*, 73:072003, 2006.
4. T. Aoyama et al. The anomalous magnetic moment of the muon in the Standard Model. *Phys. Rept.*, 887:1–166, 2020.
5. Naohito Saito. A novel precision measurement of muon  $g-2$  and EDM at J-PARC. *AIP Conf. Proc.*, 1467:45–56, 2012.
6. Tatsumi Aoyama, Masashi Hayakawa, Toichiro Kinoshita, and Makiko Nio. Complete Tenth-Order QED Contribution to the Muon  $g - 2$ . *Phys. Rev. Lett.*, 109:111808, 2012.
7. Andrzej Czarnecki, William J. Marciano, and Arkady Vainshtein. Refinements in electroweak contributions to the muon anomalous magnetic moment. *Phys. Rev.*, D67:073006, 2003. [Erratum: *Phys. Rev.* **D73**, 119901 (2006)].
8. C. Gnendiger, D. Stöckinger, and H. Stöckinger-Kim. The electroweak contributions to  $(g - 2)_\mu$  after the Higgs boson mass measurement. *Phys. Rev.*, D88:053005, 2013.
9. Tatsumi Aoyama, Toichiro Kinoshita, and Makiko Nio. Theory of the Anomalous Magnetic Moment of the Electron. *Atoms*, 7(1):28, 2019.
10. M. Davier, A. Hoecker, B. Malaescu, and Z. Zhang. A new evaluation of the hadronic vacuum polarisation contributions to the muon anomalous magnetic moment and to  $\alpha(m_Z^2)$ . *Eur. Phys. J.*, C80(3):241, 2020. [Erratum: *Eur. Phys. J.* **C80**, 410 (2020)].
11. Alexander Keshavarzi, Daisuke Nomura, and Thomas Teubner. The  $g-2$  of charged leptons,  $\alpha(M_Z^2)$  and the hyperfine splitting of muonium. *Phys. Rev.*, D101:014029, 2020.
12. Pere Masjuan and Pablo Sánchez-Puertas. Pseudoscalar-pole contribution to the  $(g_\mu - 2)$ : a rational approach. *Phys. Rev.*, D95(5):054026, 2017.
13. Pablo Roig and Pablo Sánchez-Puertas. Axial-vector exchange contribution to the hadronic light-by-light piece of the muon anomalous magnetic moment. *Phys. Rev.*, D101(7):074019, 2020.
14. A. Guevara, P. Roig, and J. J. Sanz-Cillero. Pseudoscalar pole light-by-light contributions to the muon  $(g - 2)$  in Resonance Chiral Theory. *JHEP*, 06:160, 2018.
15. P. Roig, A. Guevara, and G. López Castro.  $VV'P$  form factors in resonance chiral theory and the  $\pi - \eta - \eta'$  light-by-light contribution to the muon  $g - 2$ . *Phys. Rev. D*, 89(7):073016, 2014.
16. Igor Danilkin, Christoph Florian Redmer, and Marc Vanderhaeghen. The hadronic light-by-light contribution to the muon's anomalous magnetic moment. *Prog. Part. Nucl. Phys.*, 107:20–68, 2019.
17. Gilberto Colangelo, Martin Hoferichter, Massimiliano Procura, and Peter Stoffer. Dispersion relation for hadronic light-by-light scattering: two-pion contributions. *JHEP*, 04:161, 2017.
18. Pere Masjuan, Pablo Roig, and Pablo Sanchez-Puertas. The interplay of transverse degrees of freedom and axial-vector mesons with short-distance constraints in  $g - 2$ . *J. Phys. G*, 49(1):015002, 2022.
19. J. A. Miranda and P. Roig. New  $\tau$ -based evaluation of the hadronic contribution to the vacuum polarization piece of the muon anomalous magnetic moment. *Phys. Rev. D*, 102:114017, 2020.
20. Craig D. Roberts and Anthony G. Williams. Dyson-Schwinger equations and their application to hadronic physics. *Prog. Part. Nucl. Phys.*, 33:477–575, 1994.
21. Christian S. Fischer. QCD at finite temperature and chemical potential from Dyson–Schwinger equations. *Prog. Part. Nucl. Phys.*, 105:1–60, 2019.
22. Helios Sanchis-Alepuz and Richard Williams. Recent developments in bound-state calculations using the Dyson–Schwinger and Bethe–Salpeter equations. *Comput. Phys. Commun.*, 232:1–21, 2018.
23. Khepani Raya, Zhu-Fang Cui, Lei Chang, Jose-Manuel Morgado, Craig D. Roberts, and Jose Rodriguez-Quintero. Revealing pion and kaon structure via generalised parton distributions. *Chin. Phys. C*, 46(26):013105, 2022.
24. Zhu-Fang Cui, Minghui Ding, Fei Gao, Khépani Raya, Daniele Binosi, Lei Chang, Craig D Roberts, Jose Rodríguez-Quintero, and Sebastian M Schmidt. Kaon and pion parton distributions. *Eur. Phys. J. C*, 80(11):1064, 2020.
25. Khépani Raya, Lei Chang, Minghui Ding, Daniele Binosi, and Craig D Roberts. Unveiling the structure of pseudoscalar mesons. In *18th International Conference on Hadron Spectroscopy and Structure*, pages 565–569, 2020.
26. Minghui Ding, Khépani Raya, Daniele Binosi, Lei Chang, Craig D Roberts, and Sebastian M Schmidt. Drawing insights from pion parton distributions. *Chin. Phys. C*, 44(3):031002, 2020.
27. Si-xue Qin, Craig D Roberts, and Sebastian M Schmidt. Spectrum of light- and heavy-baryons. *Few Body Syst.*, 60(2):26, 2019.
28. Gernot Eichmann, Helios Sanchis-Alepuz, Richard Williams, Reinhard Alkofer, and Christian S. Fischer. Baryons as relativistic three-quark bound states. *Prog. Part. Nucl. Phys.*, 91:1–100, 2016.
29. K. Raya, L. Chang, A. Bashir, J. J. Cobos-Martinez, L. X. Gutiérrez-Guerrero, C. D. Roberts, and P. C. Tandy. Structure of the neutral pion and its electromagnetic transition form factor. *Phys. Rev. D*, 93(7):074017, 2016.
30. L. Chang, I. C. Cloët, C. D. Roberts, S. M. Schmidt, and P. C. Tandy. Pion electromagnetic form factor at spacelike momenta. *Phys. Rev. Lett.*, 111(14):141802, 2013.
31. Lei Chang, I. C. Cloet, J. J. Cobos-Martinez, C. D. Roberts, S. M. Schmidt, and P. C. Tandy. Imaging dynamical chiral symmetry breaking: pion wave function on the light front. *Phys. Rev. Lett.*, 110(13):132001, 2013.
32. Gernot Eichmann. Nucleon electromagnetic form factors from the covariant Faddeev equation. *Phys. Rev. D*, 84:014014, 2011.

33. Ángel Miramontes, Adnan Bashir, Khépani Raya, and Pablo Roig. Pion and Kaon box contribution to  $a_\mu^{\text{HLbL}}$ . 12 2021.
34. Khépani Raya, Adnan Bashir, and Pablo Roig. Contribution of neutral pseudoscalar mesons to  $a_\mu^{\text{HLbL}}$  within a Schwinger-Dyson equations approach to QCD. *Phys. Rev. D*, 101(7):074021, 2020.
35. Gernot Eichmann, Christian S. Fischer, Esther Weil, and Richard Williams. Single pseudoscalar meson pole and pion box contributions to the anomalous magnetic moment of the muon. *Phys. Lett. B*, 797:134855, 2019. [Erratum: *Phys.Lett.B* 799, 135029 (2019)].
36. Gernot Eichmann, Christian S. Fischer, and Richard Williams. Kaon-box contribution to the anomalous magnetic moment of the muon. *Phys. Rev.*, D101(5):054015, 2020.
37. Gernot Eichmann, Christian S. Fischer, Walter Heupel, and Richard Williams. The muon g-2: Dyson-Schwinger status on hadronic light-by-light scattering. *AIP Conf. Proc.*, 1701(1):040004, 2016.
38. Tobias Goetze, Christian S. Fischer, and Richard Williams. Hadronic light-by-light scattering in the muon g-2: a Dyson-Schwinger equation approach. *Phys. Rev. D*, 83:094006, 2011. [Erratum: *Phys.Rev.D* 86, 099901 (2012)].
39. Si-xue Qin and Craig D Roberts. Impressions of the Continuum Bound State Problem in QCD. *Chin. Phys. Lett.*, 37(12):121201, 2020.
40. Daniele Binosi, Lei Chang, Joannis Papavassiliou, Si-Xue Qin, and Craig D. Roberts. Symmetry preserving truncations of the gap and Bethe-Salpeter equations. *Phys. Rev. D*, 93(9):096010, 2016.
41. Luis Albino, Adnan Bashir, Bruno El-Bennich, Eduardo Rojas, Fernando E. Serna, and Roberto Correa da Silveira. The impact of transverse Slavnov-Taylor identities on dynamical chiral symmetry breaking. *JHEP*, 11:196, 2021.
42. M. Atif Sultan, Khépani Raya, Faisal Akram, Adnan Bashir, and Bilal Masud. Effect of the quark-gluon vertex on dynamical chiral symmetry breaking. *Phys. Rev. D*, 103(5):054036, 2021.
43. L. Albino, A. Bashir, L. X. Gutiérrez Guerrero, B. El Bennich, and E. Rojas. Transverse Takahashi Identities and Their Implications for Gauge Independent Dynamical Chiral Symmetry Breaking. *Phys. Rev. D*, 100(5):054028, 2019.
44. Zanbin Xing, Khépani Raya, and Lei Chang. Quark anomalous magnetic moment and its effects on the  $\rho$  meson properties. *Phys. Rev. D*, 104(5):054038, 2021.
45. Si-Xue Qin, Craig D. Roberts, and Sebastian M. Schmidt. Ward-Green-Takahashi identities and the axial-vector vertex. *Phys. Lett. B*, 733:202–208, 2014.
46. Mandar S. Bhagwat, Lei Chang, Yu-Xin Liu, Craig D. Roberts, and Peter C. Tandy. Flavour symmetry breaking and meson masses. *Phys. Rev. C*, 76:045203, 2007.
47. A. Bender, Craig D. Roberts, and L. Von Smekal. Goldstone theorem and diquark confinement beyond rainbow ladder approximation. *Phys. Lett. B*, 380:7–12, 1996.
48. Yin-Zhen Xu, Daniele Binosi, Zhu-Fang Cui, Bo-Lin Li, Craig D Roberts, Shu-Sheng Xu, and Hong Shi Zong. Elastic electromagnetic form factors of vector mesons. *Phys. Rev. D*, 100(11):114038, 2019.
49. Fernando E. Serna, Chen Chen, and Bruno El-Bennich. Interplay of dynamical and explicit chiral symmetry breaking effects on a quark. *Phys. Rev. D*, 99(9):094027, 2019.
50. Lei Chang, Yu-Bin Liu, Khépani Raya, J. Rodríguez-Quintero, and Yi-Bo Yang. Linking continuum and lattice quark mass functions via an effective charge. *Phys. Rev. D*, 104(9):094509, 2021.
51. Si-xue Qin, Lei Chang, Yu-xin Liu, Craig D. Roberts, and David J. Wilson. Interaction model for the gap equation. *Phys. Rev. C*, 84:042202, 2011.
52. Minghui Ding, Khepani Raya, Adnan Bashir, Daniele Binosi, Lei Chang, Muyang Chen, and Craig D. Roberts.  $\gamma^* \gamma \rightarrow \eta, \eta'$  transition form factors. *Phys. Rev. D*, 99(1):014014, 2019.
53. Pieter Maris and Peter C. Tandy. The Quark photon vertex and the pion charge radius. *Phys. Rev. C*, 61:045202, 2000.
54. Pieter Maris and Peter C. Tandy. The pi, K+, and K0 electromagnetic form-factors. *Phys. Rev. C*, 62:055204, 2000.
55. Pieter Maris and Peter C. Tandy. Electromagnetic transition form-factors of light mesons. *Phys. Rev. C*, 65:045211, 2002.
56. Ángel S. Miramontes and Hèlios Sanchis-Alepuz. On the effect of resonances in the quark-photon vertex. *Eur. Phys. J. A*, 55(10):170, 2019.
57. Ángel S. Miramontes, Hèlios Sanchis Alepuz, and Reinhard Alkofer. Elucidating the effect of intermediate resonances in the quark interaction kernel on the timelike electromagnetic pion form factor. *Phys. Rev. D*, 103(11):116006, 2021.
58. R. A. Williams, C. R. Ji, and S. R. Cotanch. Kinematically accessible vector meson resonance enhancements in p (K-, e+ e-) Lambda, Sigma0, Lambda (1405). *Phys. Rev. C*, 48:1318–1322, 1993.
59. G. Ramalho and M. T. Peña.  $\gamma^* N \rightarrow N^*(1520)$  form factors in the timelike regime. *Phys. Rev. D*, 95(1):014003, 2017.
60. Carlos Granados, Stefan Leupold, and Elisabetta Perotti. The electromagnetic Sigma-to-Lambda hyperon transition form factors at low energies. *Eur. Phys. J. A*, 53(6):117, 2017.
61. K. Raya, L. X. Gutiérrez-Guerrero, A. Bashir, L. Chang, Z. F. Cui, Y. Lu, C. D. Roberts, and J. Segovia. Dynamical diquarks in the  $\gamma^{(*)} p \rightarrow N(1535)\frac{1}{2}^-$  transition. *Eur. Phys. J. A*, 57(9):266, 2021.
62. Pieter Maris and Peter C. Tandy. Bethe-Salpeter study of vector meson masses and decay constants. *Phys. Rev. C*, 60:055214, 1999.
63. Gernot Eichmann, Christian S. Fischer, Esther Weil, and Richard Williams. On the large- $Q^2$  behavior of the pion transition form factor. *Phys. Lett. B*, 774:425–429, 2017.
64. Marc Knecht and Andreas Nyffeler. Hadronic light by light corrections to the muon g-2: The Pion pole contribution. *Phys. Rev. D*, 65:073034, 2002.
65. Khepani Raya, Minghui Ding, Adnan Bashir, Lei Chang, and Craig D. Roberts. Partonic structure of neutral pseudoscalars via two photon transition form factors. *Phys. Rev. D*, 95(7):074014, 2017.
66. Chao Shi, Lei Chang, Craig D. Roberts, Sebastian M. Schmidt, Peter C. Tandy, and Hong-Shi Zong. Flavour symmetry breaking in the kaon parton distribution amplitude. *Phys. Lett. B*, 738:512–518, 2014.



67. E. B. Dally et al. DIRECT MEASUREMENT OF THE NEGATIVE KAON FORM-FACTOR. *Phys. Rev. Lett.*, 45:232–235, 1980.
68. S. R. Amendolia et al. A Measurement of the Kaon Charge Radius. *Phys. Lett. B*, 178:435–440, 1986.
69. S. R. Amendolia et al. A Measurement of the Space - Like Pion Electromagnetic Form-Factor. *Nucl. Phys. B*, 277:168, 1986.
70. H. P. Blok et al. Charged pion form factor between  $Q^2=0.60$  and  $2.45 \text{ GeV}^2$ . I. Measurements of the cross section for the  $^1\text{H}(e, e'\pi^+)n$  reaction. *Phys. Rev. C*, 78:045202, 2008.
71. Robert Delbourgo and Peter C. West. A Gauge Covariant Approximation to Quantum Electrodynamics. *J. Phys. A*, 10:1049, 1977.